



OPEN Stages prediction of Alzheimer's disease with shallow 2D and 3D CNNs from intelligently selected neuroimaging data

Jalees ur Rahman¹, Muhammad Hanif¹, Obaid ur Rehman², Usman Haider³, Saeed Mian Qaisar^{4,5}✉ & Paweł Pławiak^{6,7}✉

Detection of Alzheimer's Disease (AD) is critical for successful diagnosis and treatment, involving the common practice of screening for Mild Cognitive Impairment (MCI). However, the progressive nature of AD makes it challenging to identify its causal factors. Modern diagnostic workflows for AD use cognitive tests, neurological examinations, and biomarker-based methods, e.g., cerebrospinal fluid (CSF) analysis and positron emission tomography (PET) imaging. While these methods are effective, non-invasive imaging techniques like Magnetic Resonance Imaging (MRI) are gaining importance. Deep Learning (DL) approaches for evaluating alterations in brain structure have focused on combining MRI and Convolutional Neural Networks (CNNs) within the spatial architecture of DL. This combination has garnered significant research interest due to its remarkable effectiveness in automating feature extraction across various multilayer perceptron models. Despite this, MRI's noisy and multidimensional nature requires an intelligent preprocessing pipeline for effective disease prediction. Our study aims to detect different stages of AD from the multidimensional neuroimaging data obtained through MRI scans using 2D and 3D CNN architectures. The proposed preprocessing pipeline comprises skull stripping, spatial normalization, and smoothing. It is followed by a novel and efficient pixel count-based frame selection and cropping approach, which renders a notable dimension reduction. Furthermore, the learnable resizer method is applied to enhance the image quality while resizing the data. Finally, the proposed shallow 2D and 3D CNN architectures extract spatio-temporal attributes from the segmented MRI data. Furthermore, we merged both the CNNs for further comparative analysis. Notably, 2D CNN achieved a maximum accuracy of 93%, while 3D CNN reported the highest accuracy of 96.5%.

Keywords Alzheimer's disease, Convolutional neural network, Deep learning, Frames selection, Learnable resizer, Magnetic resonance imaging, Multidimensional data, Preprocessing

Alzheimer's Disease (AD) is an irretrievable, progressive, and chronic neurodegenerative disorder clinically expressed by cognitive dysfunction, amnesia, and steady loss of various brain functions and everyday living independent actions¹. The number of AD patients is anticipated to grow worldwide from the existing 47 million to 152 million by the end of 2050, which causes far-reaching medical, social, and economic aftereffects². The pathogenesis of AD remains unexplained, and the available therapies cannot cure it or stop its progression completely. AD detection by Mild Cognitive Impairment (MCI) screening is critical for successful care policies and actions to counter further disease deterioration. Magnetic Resonance Imaging (MRI) analyzes the structural changes in the brain caused by AD, Mild Cognitive Impairment (MCI), and Cognitively Normal (CN)

¹Faculty of Computer Science and Engineering, Ghulam Ishaq Khan Institute of Engineering Sciences and Technology, Topi, Pakistan. ²Faculty of Computer Science and Information Technology, University of Malaya, Kuala Lumpur, Malaysia. ³Department of AI & DS, FAST School of Computing, National University of Computer and Emerging Sciences, Islamabad, Pakistan. ⁴College of Engineering and Technology, American University of the Middle East, Egaila, Kuwait. ⁵Electrical and Computer Engineering Department, Effat University, 21478 Jeddah, Saudi Arabia. ⁶Department of Computer Science, Faculty of Computer Science and Telecommunications, Cracow University of Technology, Warszawska 24, 31-155 Krakow, Poland. ⁷Institute of Theoretical and Applied Informatics, Polish Academy of Sciences, Bałtycka 5, 44-100 Gliwice, Poland. ✉email: saeed.qaisar@aum.edu.kw; plawiak@pk.edu.pl

manifestation. Neuroimaging helps in visualizing structural brain changes. Figure 1 demonstrates the brain changes where the ventricle enlargement and hippocampal size can be observed in the sample MRI images (AD brain with cortical atrophy is compared with the MRI image of MCI and CN). It is clear that the brain texture changes with the progression of AD disease (CN to MCI to AD).

Neuroimaging biomarkers have been employed in earlier research to automatically predict various phases of AD or the progression of AD^{3–5}. These investigations use MRI images heavily because of their affordable price and excellent resolution. The MRI images have been analyzed using a range of Machine Learning (ML) frameworks, including Random Forest (RF), Boosting Techniques, and the Support Vector Machine (SVM), to identify AD⁶ automatically. However, current machine learning models typically require a deliberate selection of previously established brain Regions of Interest (ROI). These are predicated on the representations of known MRI features^{7,8}. Additionally, a manual ROI assortment may contain subjective inaccuracies⁸. This is particularly the case when there is an insufficient understanding of the conclusive MRI biomarkers. In such scenarios, the pre-assorted ROIs are expected not to enclose all the potentially valuable indications to categorize the AD.

Early detection of AD can lead to a proper cure. Several solutions have been presented in this context using the classical image processing approaches^{8,9}, ML methods⁷, and the most advanced Deep Learning (DL) models^{4,5}. Classical approaches are focused on the protein side detection of the disease, which is limited to detecting AD with high confidence⁹. On the other hand, ML methods are automated ways to detect AD with as high possible confidence and probability⁶ as possible. A simple workflow for the detection of any disease, especially AD, consists of (i) data acquisition, (ii) data preprocessing, (iii) features selection or dimension reduction, (iv) model selection, (v) training, (vi) validation, (vii) testing, and (viii) evaluation. Traditional ML algorithms rely on information collected from the data rather than applying it to raw data, necessitating much work and extensive domain knowledge¹⁰. The selection of data features and information significantly impacts the classification framework's accuracy, sensitivity, and specificity, among other aspects. Moreover, the number of parameters in the ML methods is much higher, and single-subject neuroimaging data has millions of dimensions. On the other hand, the DL-based approaches take their cues directly from the input data. The handcrafted feature selection in ML is overcome by automated and self-learning-based feature selection with DL. The DL methods have multiple layers that can automate the feature extraction process by learning to turn the raw data into a more composite representation at each layer in a subsequent fashion⁵.

Attention mechanisms are crucial in deep learning architectures, particularly in tasks involving sequential or spatial data. These mechanisms enable the model to selectively focus on specific parts of the input data, assigning varying degrees of importance to different elements¹¹. In the case of medical imaging, the attention mechanisms can enhance the model's ability to identify relevant features in a region-specific manner¹². The mechanism has recently been used to detect AD from MRI modalities because MRI scans provide highly detailed and spatially complex information about the brain^{13–15}. Attention mechanisms allow the model to focus on specific ROIs within the brain, potentially capturing subtle patterns or abnormalities associated with AD.

The more cutting-edge approaches, including stacked auto-encoders (SAE)¹⁶, deep belief networks (DBNs)¹⁷, convolutional neural networks (CNNs)¹⁸, recurrent neural networks (RNNs)¹⁹, and so on, are characterized by deep learning. These techniques modify the data's low-level properties to create an abstract or high-level representation of the learning systems¹⁶. In this²⁰, a dual-tree complex wavelet transform-based approach is used to extract features from the input, after which a feed-forward neural network (FDNN) is used for classification. Convolutional layers make up the CNN, a deep multilayer artificial neural network (ANN) that enables a model to extract feature maps acquired from the product of inputs and kernels, enabling the detection of patterns. Additionally, CNNs have demonstrated excellent feature categorization accuracy^{21–23}. Two types of CNN architectures for AD classification are 2D and 3D CNNs. Some studies have also focused on transfer learning-based pre-trained models to detect the disease, including VGG architectures²⁴. The authors have used VGG-16 to accurately classify brain MRI slices into CN, MCI, and AD in binary form. The maximum accuracy reported is for AD vs. CN, which is 98%. Similarly, AlexNet is used with transfer learning to detect the disease from healthy subjects with an accuracy of 95%²⁵. These models are limited to the pre-trained shapes and sizes of the used models, while the size and structure of neuroimaging data can be changed from person to person.

The majority of CNN designs are two-dimensional. CNN fared better in segmentation applications than other techniques like logistic regression and SVM for discrimination. It demonstrates that ML algorithms like SVM and logistic regression have lower inherent feature extraction capabilities²⁶ than CNN. The detection of neurodegenerative illnesses has been shown by the Computer-Aided Diagnosis (CAD) systems, which are based on CNNs²⁷. 2D CNN architectures, such as ResNet and GoogleNet, have achieved vital distinctions between the CN AD and MCI²¹. The Alzheimer's Disease Neuroimaging Initiative (ADNI) neuroimaging data produced highly discriminative features via ResNet-152 to detect stage (AD, MCI, and CN) progression. LeNet-5, an

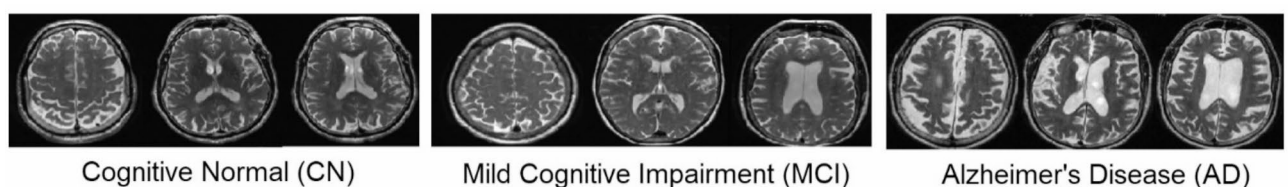


Fig. 1. Cross-sections from CN, MCI, and AD MRI images.

additional deep network and CNN architecture suggested¹⁸, separates the AD from the CN brain. Transfer learning and the VGG-16 pre-trained architecture were utilized²⁸ to classify AD, MCI, and CN into many classes. Brain slices are classified into NC, MCI, and AD using a new 2D-CNN architecture²⁹ that employs ResNet-50 with distinct activations and batch normalization. To classify the AD stages, the SegNet is proposed³⁰ to extract local information related to brain morphology. Resnet-101 executed AD, MCI, and CN classification. All the above studies have focused on the 2D architectures of CNN models. A main drawback of the 2D CNNs is they cannot detect the flow of structural changes in neuroimaging data.

However, using brain MRI images, a 3D-CNN architecture created a classifier to distinguish between the CN and AD²³. To reliably characterize the AD stages³¹, the authors have used 3D-ResNet-18 with data-augmented Resnet-18 for feature extraction. For the binary AD classification—CN vs. AD, CN vs. MCI, and AD vs. MCI—the ResNet-18 architecture is altered^{31,32}. The transfer learning technique is applied to three pre-trained CNNs, ResNet-18, ResNet-50, and ResNet-101, for MRI images' three-way classification (AD, CN, MCI). Similarly, a different deep supervised adaptive 3D-CNN³³ used 3D Convolutional autoencoder stacking to predict AD without removing the skull's structural elements. Using the ADNI dataset, a probability-based CNN fusion³⁴ employed DenseNet to identify AD stages for identifying functional changes in the neuroimaging data. The 3D Net-121 identified the AD phases with a 70% dropout rate. An ensemble of densely connected 3D-CNNs is proposed³⁵ for the AD and MCI prediction to optimize the use of extracted data. The binary classification CNN topologies (AD/MCI or MCI/CN). More research needs to be done specifically on 3D CNN architectures.

Deep learning techniques, particularly deep neural networks, have been widely used for AD detection in recent years. For example, Farooq et al. developed a deep CNN-based multi-class classification model for AD using MRI, achieving significant improvements in accuracy²¹. Likewise, Vision Transformers have been investigated for their potential in AD categorization task³⁶. Zhang et al. proposed two models namely the Convolutional Voxel Vision Transformer (CVVT) and ConvNet3D-4 for a binary AD classification. They have shown that the devised methods provide advantages in capturing global context between voxels in an MRI scan³⁶. It is shown that the CVVT and ConvNet3D-4 respectively secured 86% and 98% accuracy scores for the binary classification problem. The Optimized Vision Transformer for AD (OViTAD) further refines transformer architecture by reducing parameters and optimizing transformer input dimensions³⁷. OViTAD handles rs-fMRI and sMRI, applying complex preprocessing techniques and a majority voting system for subject-level predictions. Despite achieving high accuracy, this method flattens 3D/4D data to 2D images, potentially losing spatial context, and remains computationally expensive due to the nature of transformer models.

These aforementioned studies highlight the versatility of deep learning architectures across AD identification, paving the way for our approach to AD detection. In contrast, to previous works^{21,36}, and³⁷ our method emphasizes computational efficiency and task-specific optimization using shallow 2D and 3D CNNs. Our approach integrates domain-specific preprocessing steps, such as skull stripping, normalization, and frame selection, followed by a learnable resizer to optimize input frames dynamically. Unlike transformer-based methods, we do not rely on transfer learning or large-scale pretraining, making the model more adaptable and accessible for various clinical environments. Furthermore, our method preserves the 3D spatial structure of MRI data, improving feature extraction and maintaining contextual information critical for AD diagnosis. These differences highlight the practicality and versatility of our approach, particularly in scenarios where resources are limited or real-time inference is required.

Contribution

It is observed from the literature that researchers have focused on deep 2D CNN or 3D CNN for the automated identification of AD. Moreover, transfer learning is used for 2D CNN architectures to enhance the prediction performance and avoid the respective model's overfitting. Transfer learning has a limitation in the unchangeable dimensions of the input data and hidden layers, which might not suit all cases. Similarly, 2D CNN architectures cannot detect the temporal changes in the structures of the neuroimaging data. The 3D CNNs are suitable for detecting the temporal and spatial structural changes in the MRI data. Still, these models have limited classification accuracy due to the high and dense dimensions of the data³⁸.

In contrast, our proposed approach introduces a statistically driven frame selection method that identifies the most informative slices from MRI data, reducing computational load while preserving critical information. Furthermore, the learnable resizer method is applied to the selected MRI data to enhance the image quality for deep learning models. Additionally, we design shallow 2D and 3D CNN architectures with significantly fewer parameters than traditional models, achieving competitive accuracy with enhanced efficiency. Compared to existing few-shot object detection models, our method achieves higher accuracy with a reduced parameter count, demonstrating the effectiveness of our frame selection and model design strategies.

The primary contributions of this work are:

- Devising an efficient frame selection and cropping-based dimensions reduction method. It statistically selects the most informative slices and segments based on the pixel count, ensuring that critical features are retained while reducing the computational cost and latency. Moreover, it diminishes the model's overfitting and underfitting.
- The selected frames are resized with the help of the learnable resizer instead of interpolation methods.
- Achieving a 31.1% reduction in dataset size from preprocessed frames and a striking 92.65% reduction from raw data, highlighting its substantial efficiency for Deep Learning (DL) applications in AD detection.
- Proposing the shallow 3D and 2D architectures rather than using the known CNN deep models to enhance the detection results of all the three stages of the AD, namely the CN, MCI, and AD.
- We reduced the number of parameters by ~33% for 2D and ~85% for 3D CNNs, respectively, while maintaining comparable or better accuracy than their counterparts.

The functioning steps are:

- (i) The ANDI dataset is used to test the method's applicability. Each intended instance contains a sagittal, coronal, and transverse view.
- (ii) Each intended image is pre-processed for enhancement and noise removal. This stage includes skull stripping, spatial normalization, smoothing, grey normalization, slicing, and resizing.
- (iii) Efficient frame selection and cropping-based dimension reductions are done using a novel approach.
- (iv) Resize the efficiently selected frames with the learnable resizer instead of using interpolation techniques.
- (v) To keep the system computationally efficient, the 3D and 2D shallow CNN architectures are employed for automated categorization.
- (vi) To avoid biases, multiple evaluation measures, accuracy, F1-score, precision, and recall are used to assess the classification performance.
- (vii) As per the author's best knowledge, the MRI multi-view imaging-based automated categorization of all the three stages of AD, the CN, MCI, and AD, is not carried out in the above-mentioned numerated manner.
- (viii) The same dataset is comprehensively compared with recent state-of-the-art methods. The proposed method achieves similar or better performance, demonstrating the technique's dependability and resilience in detecting AD through MRI image processing.
- (ix) The rest of the paper is organized as follows: Section "[Materials and methods](#)" describes the materials and methods used. Section "[Experiments and results](#)" presents and discusses the experimental settings and findings. Finally, Section "[Conclusion](#)" concludes this paper.

Materials and methods

Figure 2 illustrates the overall flow of the proposed methodology. The raw MRI data undergoes initial preprocessing to eliminate noisy data. Since the number of frames in all three MRI views is relatively high, the most informative frames are selected using the proposed dimension reduction methods. The selected and cropped frames are passed through the learnable resizer method to improve image quality and reduce computational complexity. Finally, both 2D and 3D CNN architectures are introduced.

Dataset

The ADNI database provided the MRI data that were used in the investigation^{39,40}. Three labels are included in the labeled ADNI dataset: moderate cognitive impairment (MCI), cognitive normal (CN), and Alzheimer's disease (AD). The same patient appears across multiple visits within this dataset. Approximately 7,000 NIFTI files (3D MRI scans) are available. A selection of opinions is shown in Fig. 3. We have considered T1-weighted 3-year data, which contains 2,182 NIFTI files. Each NIFTI file includes a subject's sagittal, coronal, and transverse views. There are more than 250 sequenced frames/slices for all three views of the MRI data. It is clear from Fig. 3 that the data is quite noisy. Therefore, the brain portion should be extracted from these images for further processing. Additionally, the distribution of the dataset by gender and label, along with statistics on age and number of visits, is as follows: CN: 748, MCI: 981, AD: 453, Male: 1,279, Female: 930, Average Age: 76.23, Standard Deviation of Age: 6.8, and Average Number of Visits per subject: 4.1.

Preprocessing

Preprocessing is one of the critical steps in medical imaging. The standard preprocessing pipeline of medical imaging includes the following:

- Skull stripping.
- Spatial normalization.
- Smoothing.

Using the default parameters of the CAT12 toolkit of the SPM12 toolbox (MATLAB third-party toolbox), the T1-Weighted MRI data from the ANDI in NIFTI format was preprocessed. Skull stripping, spatial normalizing, and smoothing are all part of the preprocessing pipeline, which results in MRI images that are all 3D and follow the dimensions of 121, 145, and 121, respectively, for X, Y, and Z with a spatial resolution of $(1.5 \times 1.5 \times 1.5)$ mm³/voxel. Furthermore, every voxel value in an MRI image is normalized based on its signal intensity. The initial value is split by the MRI image's real maximum value. The values obtained from this normalization fall between 0 and 1. Figure 4 displays the views that are produced following the preprocessing pipeline. Re-slicing was used to get the 3D-MRI ($121 \times 145 \times 121$), which is the total number of sagittal, coronal, and transverse views (145×121 , 121×121 , and 121×145 , respectively). Following edge padding and zero filling, the dimensions of each 2D slice were adjusted to (145×145) . Each 2D slice was squared after scaling. However, the reformatted MRI image's central and spatial resolution remained unaltered. An explanation of the entire preprocessing pipeline is presented following.

Skull stripping

The skull stripping technique is an essential field of research for applications involving brain image processing. It speeds up and improves the precision of diagnosis in various medical applications. Therefore, it serves as an initial step. Brain scans are altered to remove non-cerebral structures such as the dura, scalp, and skull. The Adaptive Probability Region-Growing (APRG) method improves the probability maps⁴¹. Currently, this approach yields the most accurate and consistent results. This study used the APRG approach to extract the skull

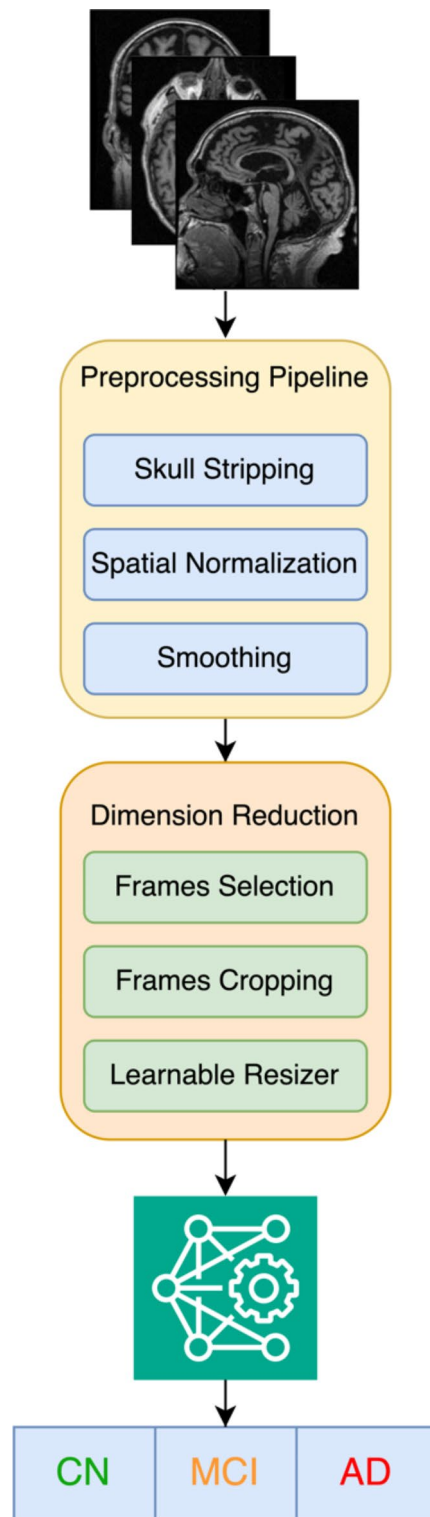


Fig. 2. The devised methodology.

from MRI data. Given the deviations of ud and ld , the upper and lower thresholds are computed to find the membership region using (1) and (2).

$$T_{upper} = mgv(n) + [ud(n) \cdot w + c(n)] \quad (1)$$

While

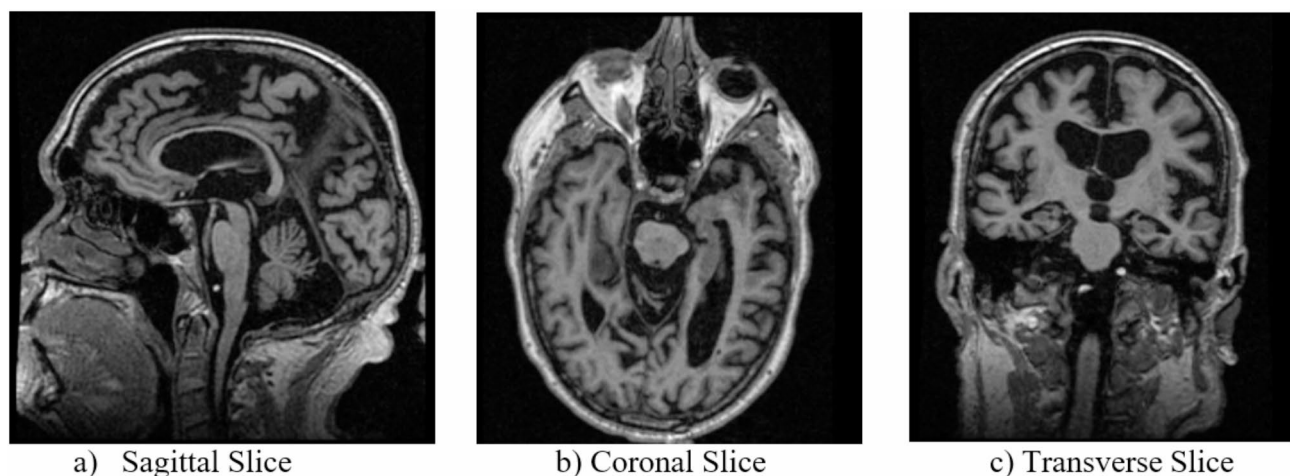


Fig. 3. Sample views of MRI images from the ADNI database.

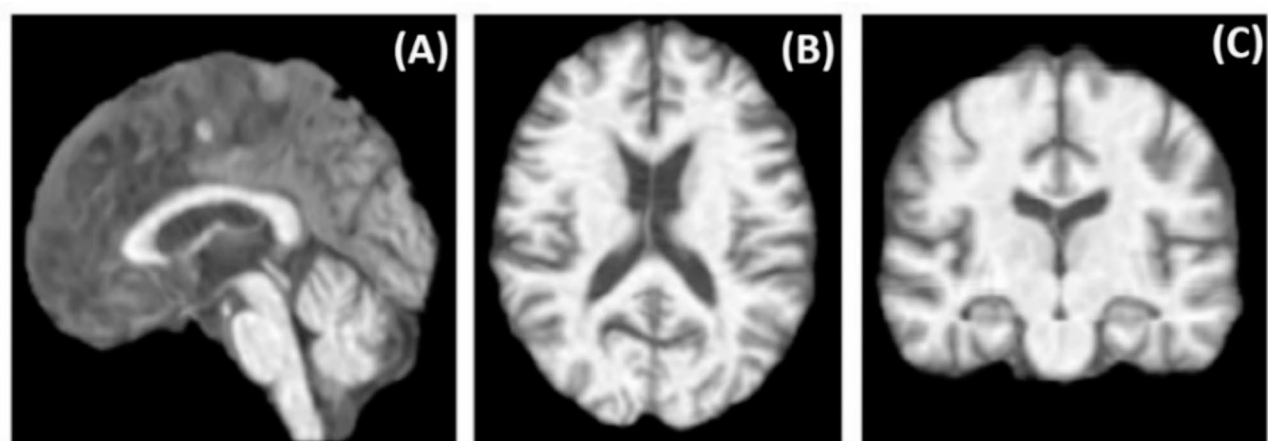


Fig. 4. MRI Preprocessed Views; (A) Sagittal Slice, (B) Coronal Slice, and (C) Transverse Slice.

for segment in Intelligently Selected Slices (ISS):

for patient in patients:

locate the first zero vector's left, right, top, and bottom

remove the intended frame's zero-valued vectors

compute mean of the trimmed image

Algorithm. Generic windows size.

$$T_{lower} = mgv(n) - [ld(n) \cdot w + c(n)] \quad (2)$$

Where n is the number of pixels used to compute the estimate.

Spatial normalization

Spatial normalization aims to modify human brain scans such that one position in a subject's brain scan corresponds to the exact location in a different brain scan. This is because human brains differ in size and shape. To be more precise, pictures from various subjects need to be spatially converted so that they all live in the same coordinate system and that anatomically relevant regions are situated similarly. To facilitate comparisons between subjects with different brain morphologies, spatial normalization is a unique type of image registration that aligns an individual's MRI image with a reference brain space. This study used the DARTEL⁴² recordings to

an existing spatial registration template; additionally, by choosing the first of six photos (iterations) of a DARTEL template, an optimal shooting strategy is used that uses an adaptive threshold and lower beginning resolutions to achieve a good balance between accuracy and calculation time.

Smoothing

Smoothing is utilized to eliminate the various noises from the MRI frames. The MRI data is sent through a Gaussian filter to cut down on noise. The finalized preprocessed frames of all three viewpoints are displayed in Fig. 2, which displays the images.

Let $I(x, y)$ represent the pixel's intensity value in the input image at coordinates (x, y) . Convolution of the input image with a Gaussian kernel, $G(x, y)$, is the process of smoothing and it is mathematically given as:

$$I_{Filter}(x, y) = (I * G)(x, y) = \sum_{i=-\infty}^{\infty} \sum_{j=-\infty}^{\infty} I(i, j) \cdot G(x - i, y - j). \quad (3)$$

In Eq. (2), $*$ is the convolution operation. $I_{Filter}(x, y)$ is the smooth image and $G(x, y)$ is given as:

$$G(x, y) = \frac{1}{2 \times \pi \times \sigma^2} \times e^{-\frac{x^2 + y^2}{2 \times \sigma^2}}. \quad (4)$$

In Eq. (4), σ is the standard deviation of the Gaussian distribution and in this study its value is selected as 0.8.

Dimension reduction

Following preprocessing, each view of the MRI scans contains nearly 150 slices. Enough calculations are required to train a CNN model on these enormous slices/frames. Additionally, redundant data could lead to a CNN becoming overfit. To lower the overall computations per MRI image, each view's frame count must be decreased. To address this problem, a recent study randomly selected 33 transverse, 50 coronal, and 40 sagittal slices—a total of 123 slices—of a subject's three-dimensional brain image⁴³.

Since it's unclear which frame has more information, the random selection of frames is not persuasive. Data loss due to random selection is a possibility. Based on the statistical analysis, the most relevant frames have been chosen for our research. First, the count of valid pixels is performed. A slice is eliminated, and the remaining frames are selected if they have fewer informative pixels than a threshold value. The following formula (5) can be used to determine the count of informative pixels.

$$I = 1 - \frac{\tilde{N}_0}{W_F \times H_F}. \quad (5)$$

Where W_F is the frame's height, H_F is its width, and \tilde{N}_0 is the total number of zeros in the same frame. For this study, 16% of the most informative frames were selected from each view, ensuring optimal data representation. This resulted in a total of ~120 carefully chosen frames per patient across all views. Statistically chosen frames led to a decrease in MRI's computational complexity. The instructive zone was varied in size in every single frame. By using the suggested algorithm, a generic average window size is determined for each patient and each of the three views (sagittal, coronal, and transverse):

The resulting slices have significantly decreased the processing of the MRI files in terms of computing complexity. Figure 5 displays an example transverse view following slice cropping.

Learnable resizer

The learnable resizer is a critical component of the proposed preprocessing pipeline, integrated to optimize the preparation of MRI frames for deep learning models. Unlike traditional resizing methods like bilinear or bicubic interpolation, the learnable resizer enhances the image specifically for machine vision tasks as shown in Fig. 6. This resizer is designed to transform the spatial dimensions and feature representation of frames dynamically. The method improves both computational efficiency and model performance. The resizer is implemented as a lightweight CNN that is trained jointly with the downstream deep learning model. It consists of multiple convolution layers and uses a task-driven resizing operation that optimizes frame dimensions without compromising critical features required for accurate diagnosis. This approach allows for more intelligent resizing to emphasize the vital brain patterns, while non-informative regions and noise are suppressed.

Deep learning (DL) models

After the data preprocessing steps, the proposed methodology is divided into two categories, i.e., 2D CNNs and 3D CNNs. Recent research used 2D CNNs, i.e., $width \times height \times number_of_frames$, for each view and merged the results⁴³. The proposed study reduces the number of hidden layers in the 2D CNNs because the frame selection reduces the input data size, as shown in Fig. 7. Furthermore, this research has applied 3D architecture as well, in which a shallow 3D CNN architecture, as shown in Fig. 8, i.e., $width \times height \times view \times number_of_frames$, is proposed and compared with 2D CNN and recent research that has used 3D CNN for the classification of AD²³. The proposed 3D CNN captures the information from all three views simultaneously.

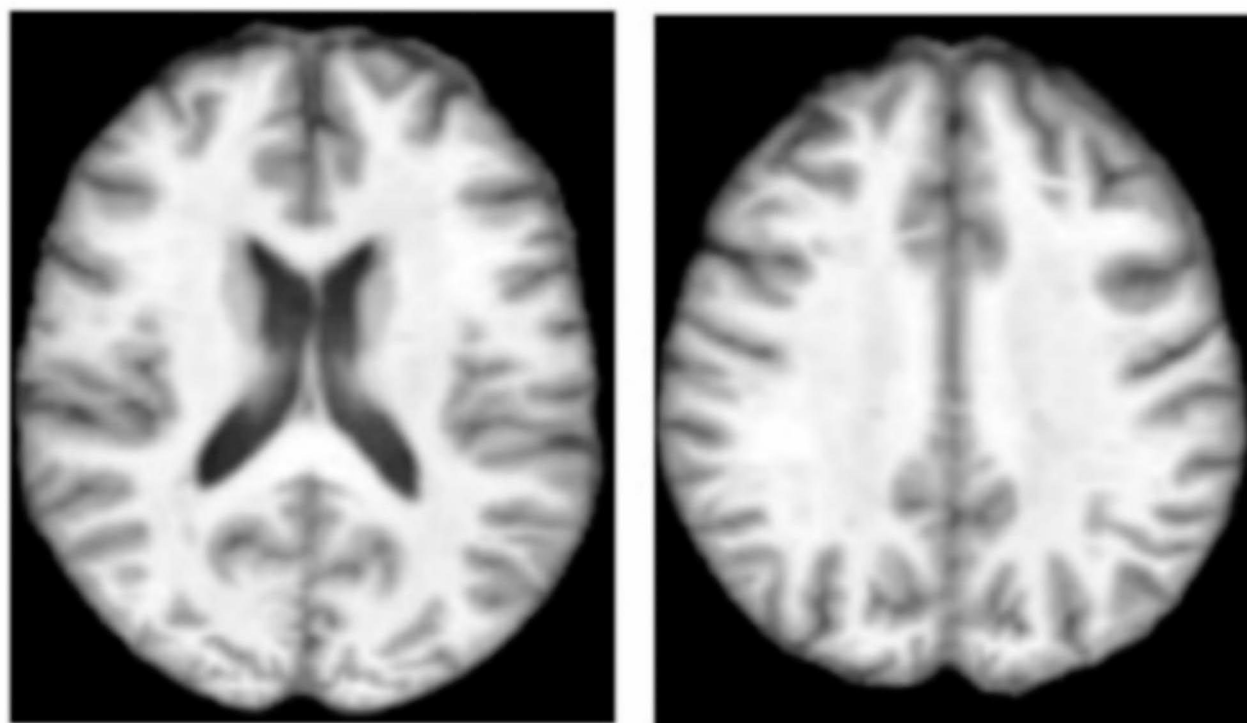


Fig. 5. Sample Transverse View of Slices.

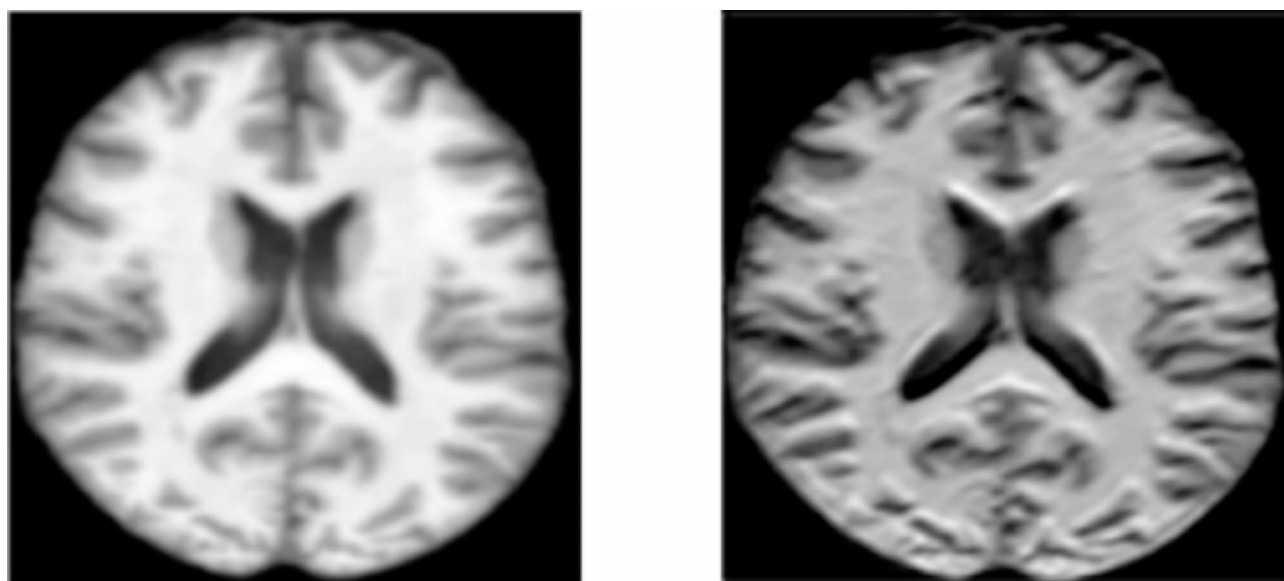


Fig. 6. Selected Transverse View (A) before learnable resizer (B) after learnable resizer.

Experiments and results

Experimental setup

As discussed in the methodology section, this research has focused on the shallow 2D- and 3D-CNN architectures to avoid the model's underfitting and overfitting. 3D CNN is further divided into three different categories belonging to the three views, i.e., coronal, sagittal, and transverse. The 2D and 3D CNN architectures are shown in Figs. 6 and 7, respectively, where C stands for the convolutional layer, P for the pooling layer, and FC for the fully connected layer. Both architectures are shallow because of intelligent frame selection and cropping compared to the counterparts. The number of parameters for each 2D CNN is 1,152,115, while 3D CNN has a

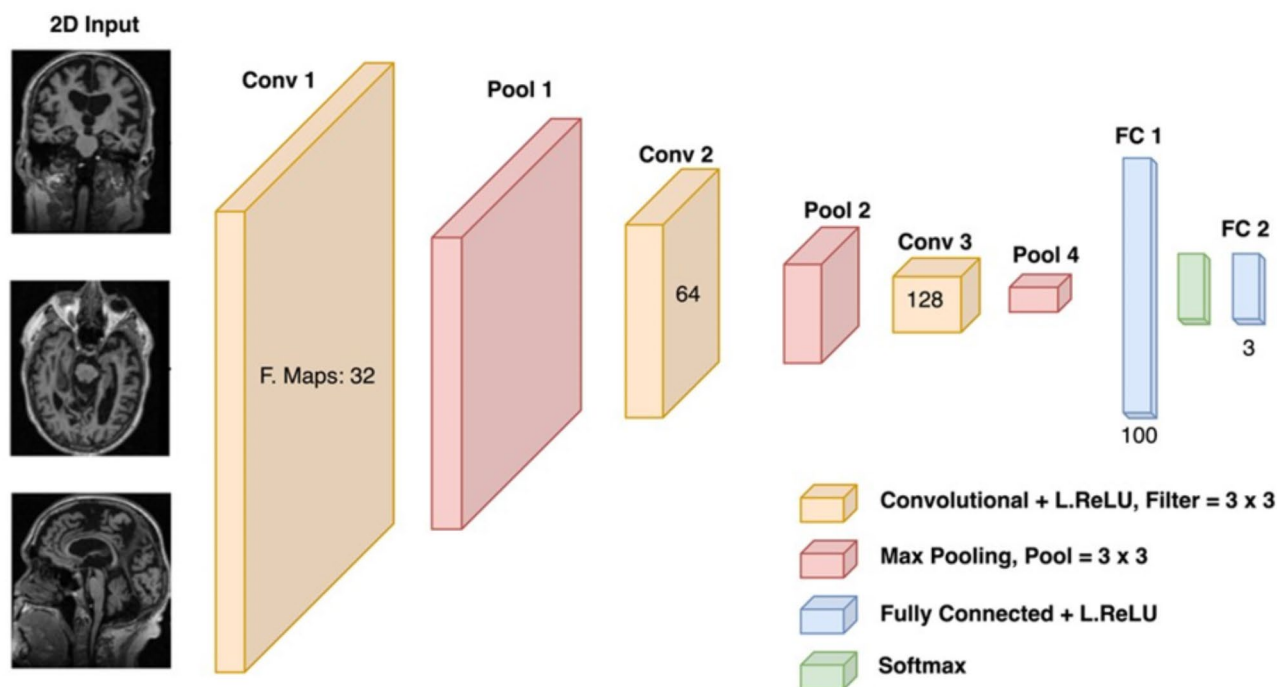


Fig. 7. 2D CNN architectures. Each view has its own CNN architecture with the same parameters.

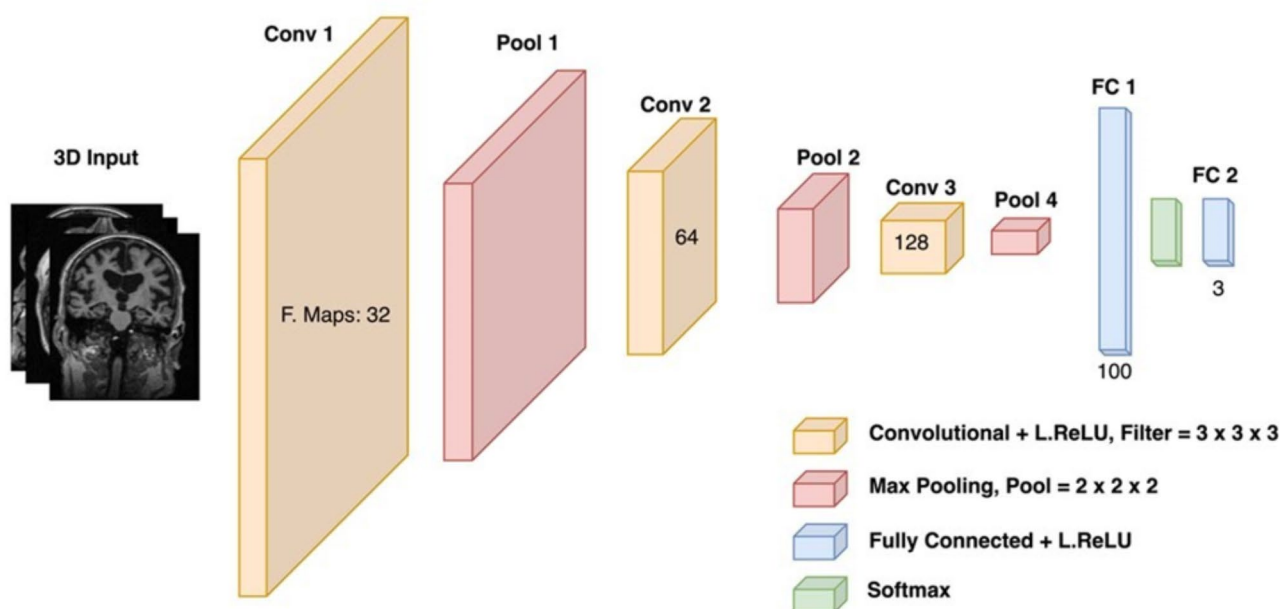


Fig. 8. 3D CNN architecture.

total of 1,091,475 parameters. Moreover, Table 1 depicts the configurations of both the models, i.e., 2D CNNs and 3D CNNs. All the models are used with the callbacks of early stopping and reduced learning rate to improve the performance of the models.

Evaluation measures

The performance parameters used in this research are reported in terms of accuracy, precision, recall, and F-measure. The equations for all four performance measures are given in Eqs. (6), (7), (8), and (9). True Positive (TP) are those instances whose ground label is true and is predicted as true, while True Negative (TN) are false and predicted as false. Moreover, False Positives (FP) is negative but predicted to be positive, while False

Parameter	Configuration	
Learning Rate	Initial Value	0.001
	Nature	Timely Decreasing (Adaptive)
	Reduction Factor	0.1
	Minimum Possible Value	0.00001
	Reduction Monitoring	Validation Accuracy
	Patient to Reduction	2 times
Stopping Criteria	Stopping Monitoring	Validation Accuracy
	Patience to Stop	4 times
	Initial Learning Rate	0.01
Weights	Trainable	Yes
	Initial Weights	Random
Training	Optimizer	Adam
	Loss	Categorical Cross Entropy
	Maximum Possible Epochs	Infinite
	Batch Size	64
	Validation Split	15%
	Performance Metric	Accuracy

Table 1. Configuration table for the proposed DL architectures.

Negatives (FN) is positive but predicted to be negative. As there are four different datasets, i.e., three 2D datasets (coronal, sagittal, and transverse) and one 3D dataset, this section has subdivided the results and described each separately.

$$\text{Precision} = \text{TP} / (\text{TP} + \text{FP}) \quad (6)$$

$$\text{Recall} = \text{TP} / (\text{TP} + \text{FN}) \quad (7)$$

$$\text{F-measure} = 2 * (\text{Recall} * \text{Precision}) / (\text{Recall} + \text{Precision}) \quad (8)$$

$$\text{Accuracy} = (\text{TP} + \text{TN}) / (\text{TP} + \text{FP} + \text{FN} + \text{TN}) \quad (9)$$

Results and discussion

2D CNN

All three views' results are compiled and reported in the subsections below, which consist of training and validation plots and confusion matrices. The number of epochs for each view differs because of the callbacks.

Coronal view

The number of epochs required to train and validate the 2D CNN model for coronal view is 31. After 31 epochs, the model automatically stops the training as the model was going to overfit, as per our proposed callbacks mentioned in Table 1. Training and validation plots for coronal view are depicted in Fig. 9, where x-axis has total epochs until model is best fit while y-axis shows the accuracy of the model in percentage. Validation plot is slightly unsmooth because the view has still some noise which causes the underfitting while training the model. Confusion Matrix (CM)-1 shows the confusion matrix compiled between the actual labels and predicted labels. The testing accuracy of the model is 92%.

	CN	MCI	AD
CN	130	12	8
MCI	6	186	4
AD	2	4	84

CM-1: Confusion Matrix of 2D CNN for coronal view.

Sagittal view

The number of epochs required to train and validate the 2D CNN model for sagittal view is 16. After 16 epochs, the model automatically stopped the training as the model was going to overfit. Training and validation plots for the sagittal view are depicted in Fig. 10. It is shown from the figure that the model validation is not that smooth in terms of accuracy, which means that the sagittal view has less information. Moreover, CM-2 shows the confusion matrix compiled between actual and predicted labels. The testing accuracy of the model is 90.4%.

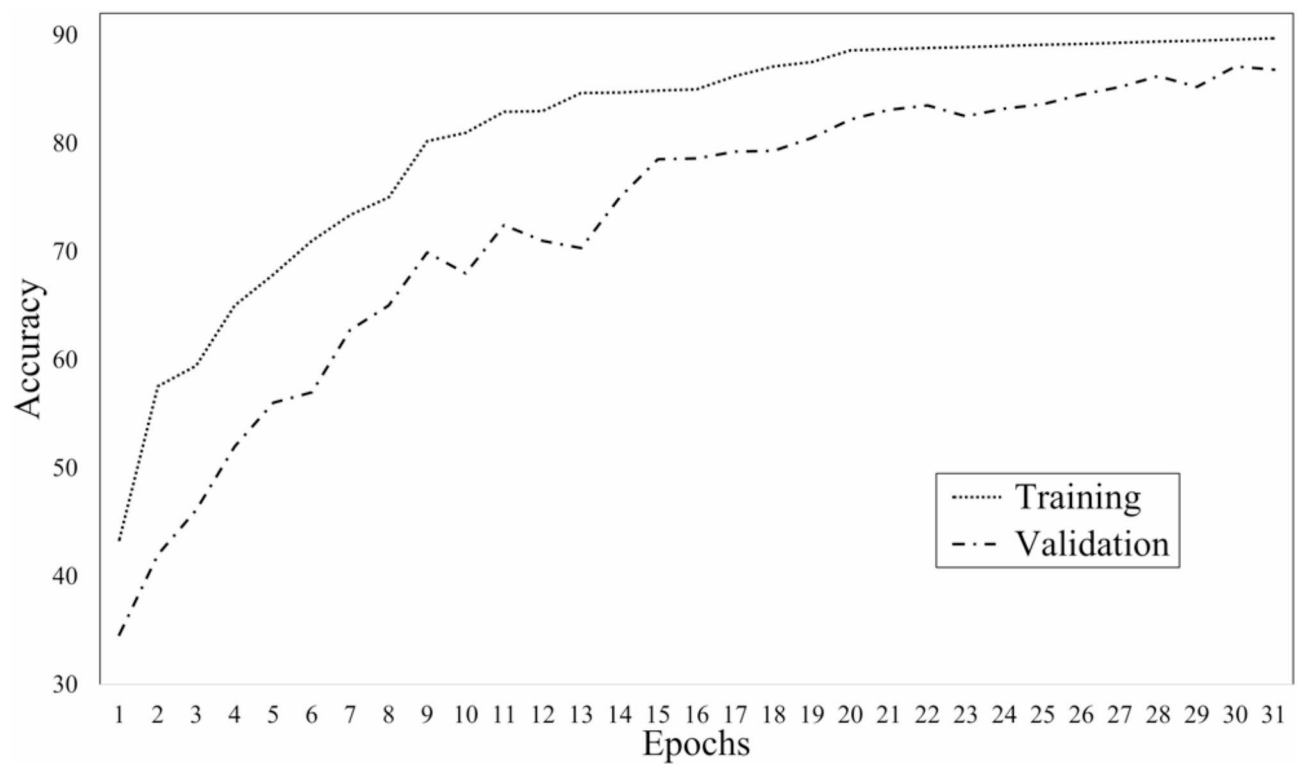


Fig. 9. Training and validation graph for coronal view (2D).

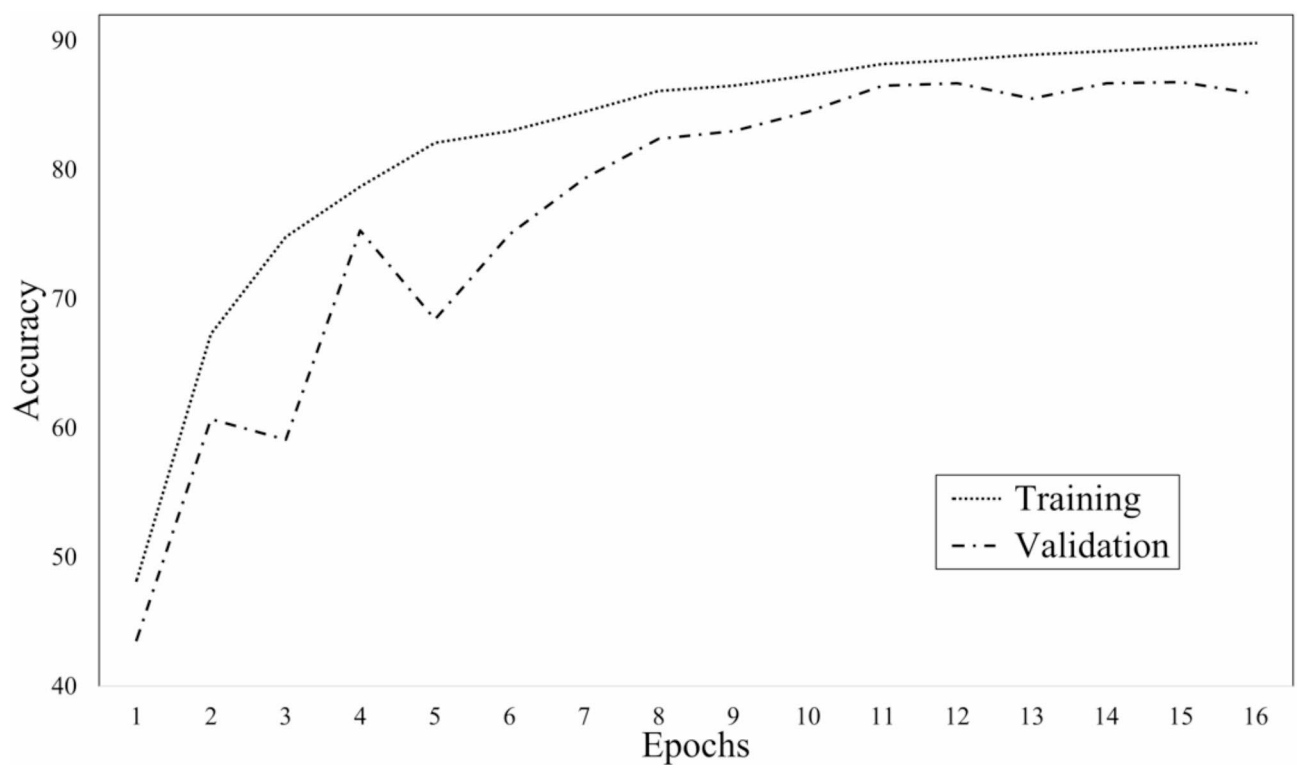


Fig. 10. Training and validation graph for sagittal view (2D).

	CN	MCI	AD
CN	129	11	10
MCI	6	181	9
AD	6	5	79

CM-2: Confusion Matrix of 2D CNN for sagittal view.

Transverse view

The number of epochs required to train and validate the 2D CNN model for the transverse view is 32. After 32 epochs, the model automatically stopped training as the model was going to overfit. Training and validation plots for the coronal view are depicted in Fig. 11. CM-3 shows the confusion matrix compiled between the actual labels and predicted labels. The testing accuracy of the model is 93%.

	CN	MCI	AD
CN	130	10	6
MCI	5	184	7
AD	3	4	83

CM-3: Confusion Matrix of 2D CNN for transverse view.

From the above three CMs, the testing accuracy of the coronal view is 92%, the sagittal view is 90.4%, and the transverse view has an accuracy of 93%. It can be seen from the results that the transverse view has much more information than the sagittal view because the transverse view has less zero value (no information) in a single subject's MRI than the sagittal view. After compiling all the results separately, the mean accuracy, precision, recall, and F-measure for all three 2D CNNs are 91.8%, 90.7%, 91.7%, and 91%, respectively.

3D CNN

After completing a set of 2D experiments, this research has suggested 3D CNN architectures along with the results. The number of epochs required to train and validate the 3D CNN model is 34 because the data is in higher dimensions than 2D. After 34 epochs, the model automatically stopped training as the model was going to overfit. Training and validation plots for 3D data are depicted in Fig. 12. CM-4 shows the confusion matrix

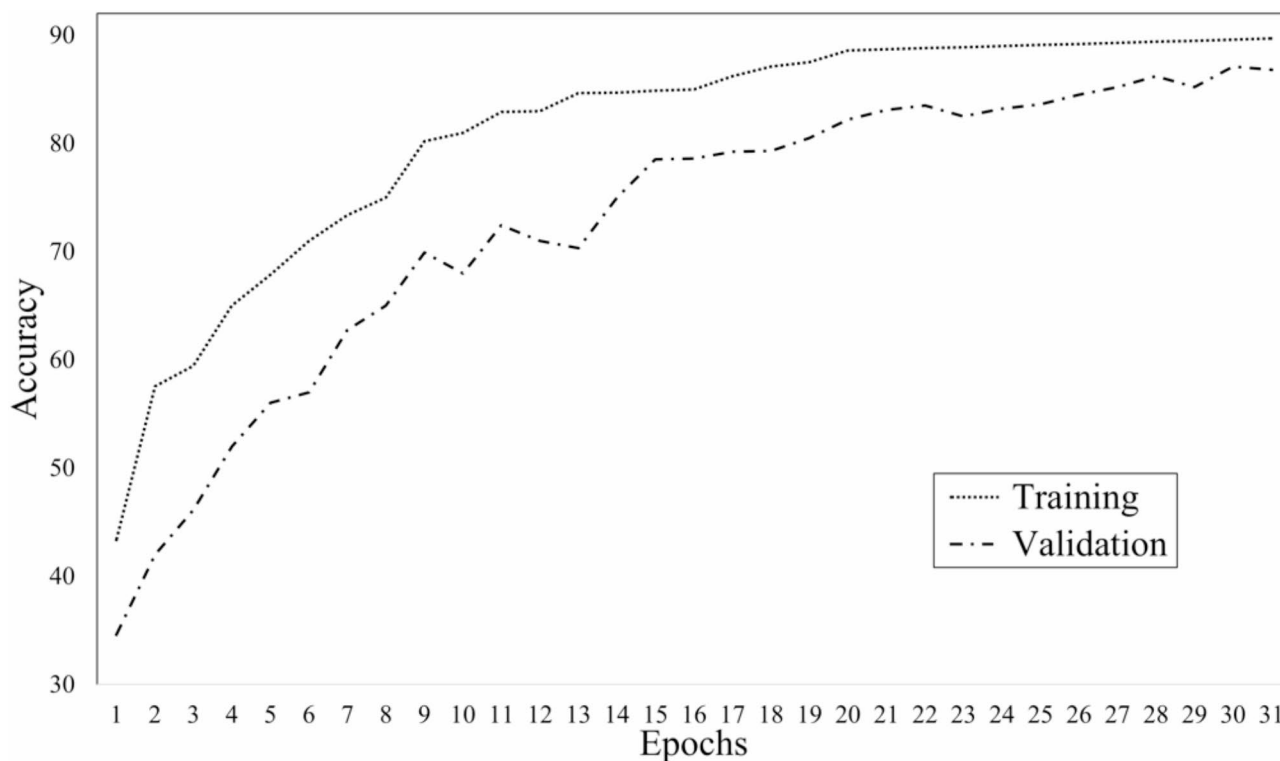


Fig. 11. Training and validation graph for transverse view (2D).

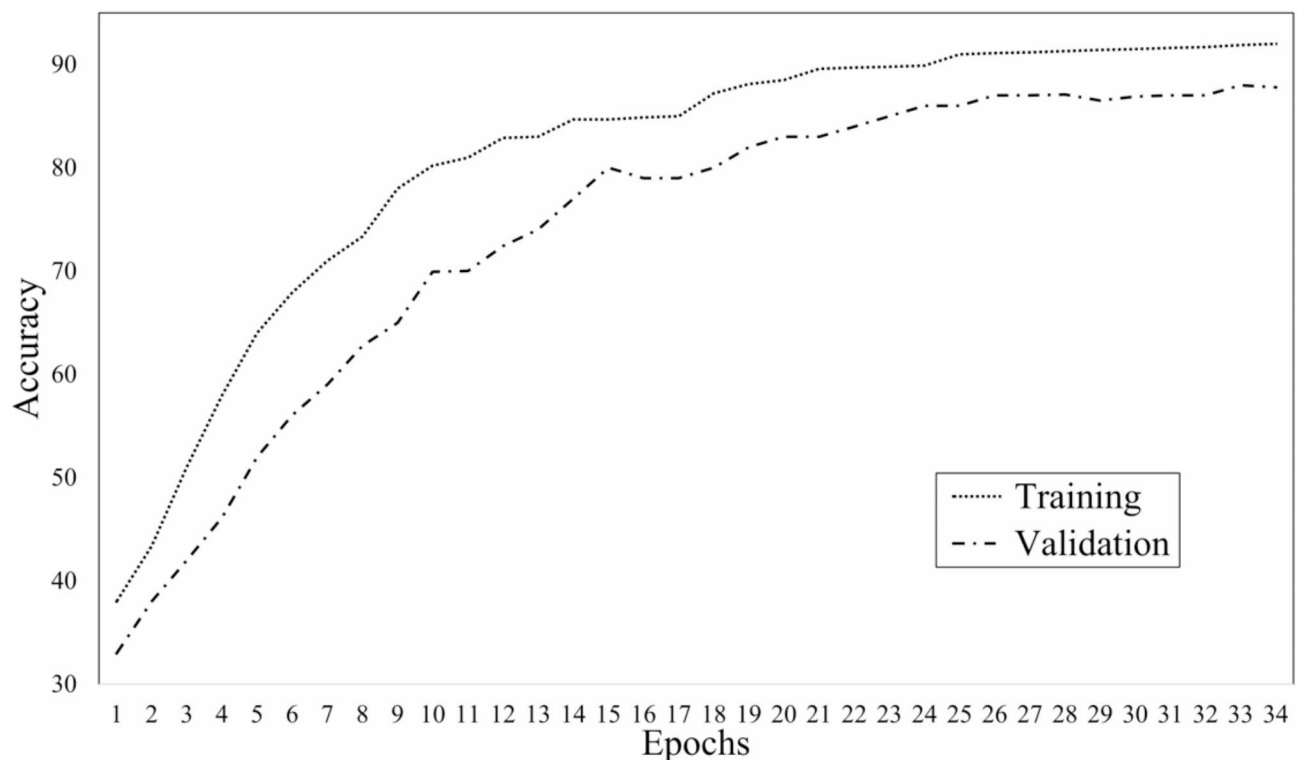


Fig. 12. Training and validation graph for 3D CNN.

compiled between the actual labels and predicted labels. Compared to the other three figures of 2D CNN, the validation plots of the 3D CNN are much smoother and diverge while training. It shows that the 3D CNN can capture the information from all three views simultaneously, which avoids the model's underfitting. Due to the high dimensions of input data for 3D CNN, it also avoided the model's overfitting compared to other 2D CNN models. The testing accuracy reported for the 3D CNN is 96.4%.

	CN	MCI	AD
CN	142	3	5
MCI	3	191	2
AD	2	1	87

CM-4: Confusion Matrix of 3D CNN.

Analysis and interpretation

From the complete set of experiments performed on 2D- and 3D-CNN architecture, this research has analyzed the fact that data size can affect the performance of any deep learning model³⁸. Figure 13 shows the overall performance between the 2D CNN architectures and the 3D CNN architecture proposed by this research. Figures 7 and 8 show that both models are shallow because of the intelligent frames' selection and cropping. Compared to 2D CNNs, 3D CNN performance is much better, and the model converges correctly because of the simultaneous extraction of features from data. In 2D views, CNN models can extract features from a single one, which is not the case in 3D data. Features from the same region are extracted in 3D CNN from all three views. That is why 3D CNN models result in ~88% precision, recall, and F-measure better than 2D views.

2D CNNs perform well but lack 3D CNNs due to the individual classification of views. Due to the side view of the brain, the sagittal view has less information than the other two views, which is why classification based on the sagittal view is low compared to the other two views. Similarly, due to the top view of the brain, the transverse view has a more informative region in the input data, which results in the best results among the other two views. The front view of the brain, coronal view, has more region than sagittal view, which results in slightly better results than sagittal. The CNN model used for the transverse view and coronal is a better fit than the sagittal view due to the less information. The fitting of CNN models depends on the number of learnable parameters in any DL model³⁸.

Table 2 compares the proposed 2D- and 3D-CNN architectures and the most relevant counterparts. The authors used 123 random frames selected from the input preprocessed data, trained all the 123 2D models separately, and then took the average of all the accuracies. It is observed that the number of parameters⁴³ has

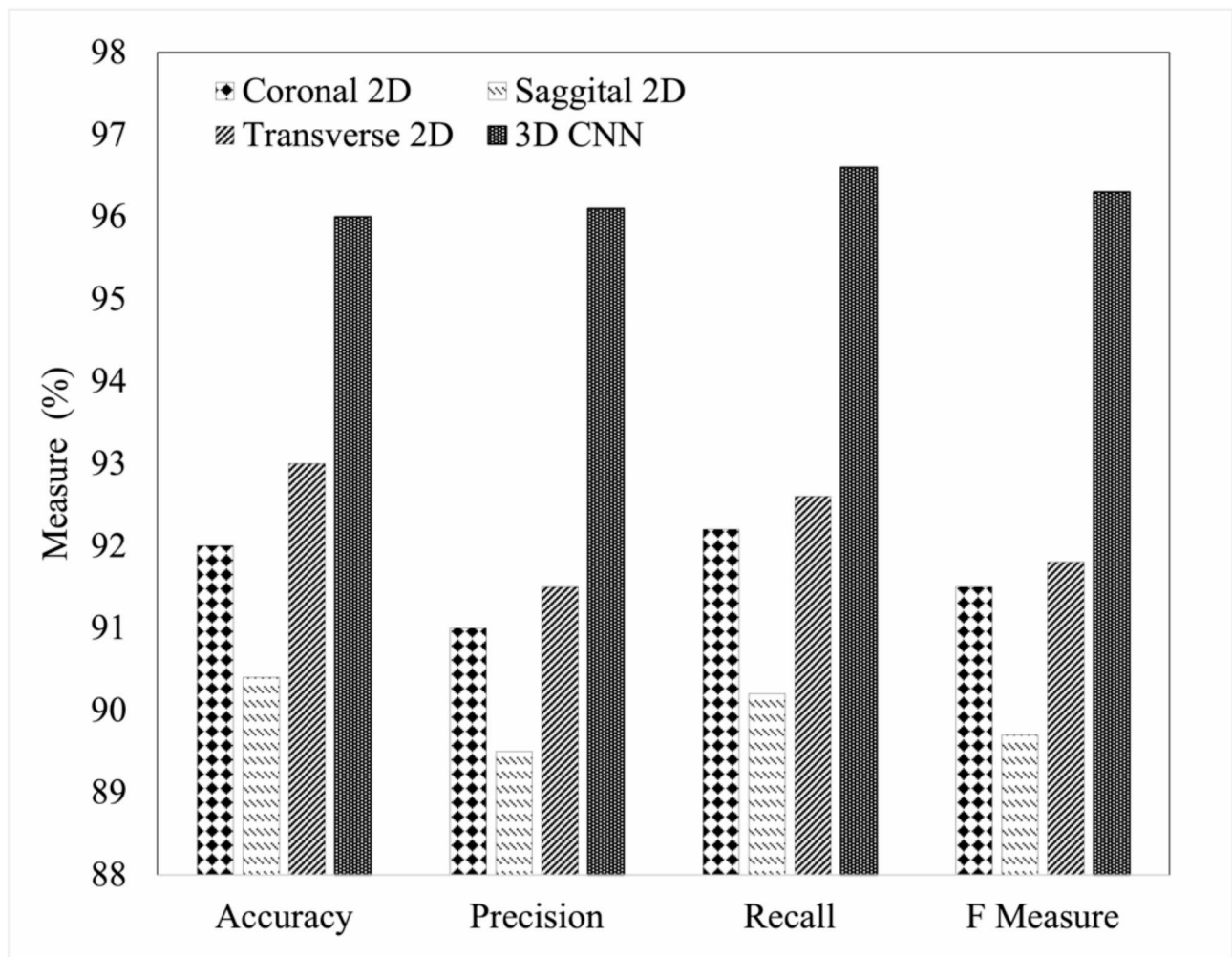


Fig. 13. Performance comparison between the proposed architectures.

Study	Architecture	No. of Subjects	Parameters	No. of Models	Accuracy (%)
⁴¹	2D CNN	509	1,227,731	123	84.05
²⁵	2D VGG-19	300	138,423,208	1	87.15
Proposed	2D CNN	2186	1,152,115	3	93
²⁴	3D CNN	988	10,467,315	1	84.57
³⁵	3D DenseNet-121	3512	7,628,484	1	84
Proposed	3D CNN	2186	1,091,475	1	96.5

Table 2. Performance comparison of the proposed architectures with counterparts.

1.227 M parameters, which is more than the 2D CNN architecture proposed by this research. Results have confirmed that the performance of the proposed model is 2+% higher than the work previously presented⁴³. Similarly, it has used a transfer learning-based 2D VGG-19 model containing 138,423,208 parameters, much more than our proposed method²⁴. Moreover, the dataset size is almost 7 times less than our selected dataset and the accuracy is 5.85% less than our proposed method. Moreover, the number of parameters is much higher than ours, and the dataset size is also much less than ours. This is the reason our proposed model has outperformed the two intended counterparts.

The 3D CNN model used in this research has fewer learnable parameters than well-known research²³. The authors have performed a set of different layer-wise experiments, and the best performance for tertiary classification, as reported by the authors, is 84.57%, almost 12% less than the proposed 3D CNN architecture. Moreover, the number of subjects is just 988, which is relatively low compared to our selected dataset. The possible reason is that the number of parameters in the proposed 3D CNN is almost 10 times less than the

models used in the literature. Similarly³⁴, it used a much larger dataset size, but the number of parameters was more significant than our proposed method, while the accuracy was less than ours. The authors have used 3D DenseNet-121 architecture to train and predict the disease. Our proposed model performance is almost 12% greater than³⁴ our intelligent frames selection and cropping, as well as the simpler CNN architecture we have proposed in this study.

The benefits of the proposed work in the context of AD detection using DL are multifaceted and significant, as outlined through our contributions and corroborated by our final results. Firstly, the devised efficient frame selection and cropping method substantially reduces the dimensionality of the dataset. This reduction achieves lower latency and computational costs and minimizes the risks of overfitting and underfitting in model training, leading to more robust and reliable diagnostic models.

Our novel approach facilitates a 31.1% reduction in dataset size from preprocessed frames and a remarkable 92.65% reduction from raw data. Such efficiency improvements are pivotal for Deep Learning applications in AD detection, where large datasets often pose significant challenges regarding storage, processing time, and computational resources. By addressing these challenges, our method enhances the accessibility and scalability of DL applications in clinical settings.

Furthermore, the study significantly lowers computational costs by approximately 33% for 2D CNNs and about 85% for 3D CNNs. This reduction is achieved without compromising the accuracy of 2D models and, notably, while improving the accuracy of 3D models. Such advancements demonstrate the effectiveness of our approach in optimizing resource utilization while maintaining, or even enhancing, diagnostic performance. Our proposal of shallow 3D and 2D architectures, as opposed to conventional deep CNN models, is particularly beneficial in enhancing the detection results across all three stages of AD, i.e., CN, MCI, and AD. This strategic choice underscores the potential of shallower architectures in capturing the nuanced features of AD progression with reduced complexity and improved interpretability.

The results of our study further validate the benefits of the proposed methods. Compared to existing studies, our proposed 2D CNN model achieved a high accuracy of 93% with a significantly larger subject pool and lower parameter count, highlighting efficiency and scalability. The proposed 3D CNN model stands out by achieving the highest accuracy of 96.5% among the compared studies, with the lowest number of parameters, illustrating the potential of our approach in setting new benchmarks for AD detection accuracy and computational efficiency. In summary, the proposed work substantially benefits detecting AD by detecting a path toward more accessible, efficient, and accurate diagnostic tools. These contributions offer the field technical promise to make early and precise AD detection more feasible in clinical practices worldwide.

Conclusion

This paper proposes a novel method for automated detection of the Alzheimer's Disease (AD) stages by processing the Magnetic Resonance Imaging (MRI). The solution is based on an effective hybridization of the preprocessing, frame selection, and cropping with shallow 2D and 3D Convolutional Neural Networks (CNNs). The preprocessing stage involved skull stripping, spatial normalization, and smoothing. Onward, the proposed pixel count-based frame selection and cropping approach is applied to the preprocessed MRI data, followed by the learnable resizer method. It renders an efficient dimension reduction. Afterward, the designed shallow 2D and 3D CNN architectures extract spatio-temporal attributes from the selected MRI data. Finally, both CNN models are evaluated for a comparative analysis. Notably, 2D CNN achieved a maximum accuracy of 93%, while 3D CNN reported the highest accuracy of 96.5%. The performance of CNNs is dependent on the input data. The cleaner and more informative the data is, the more accurate the CNN model will be. This research has concluded this phenomenon by experimental results—training on the less informative data results in overfitting CNN architectures. Similarly, a CNN with more learnable parameters can lead towards the model's overfitting and vice versa. Extracting features from data using 2D CNN architectures can lead to model underfitting compared to 3D. CNN models with higher dimensions can sometimes extract more data from different views simultaneously, which is the cause behind more than 96% accuracy.

Moreover, training and inference time for shallow CNN models and small-sized data is less than that for deeper CNN models. This is why MRI, a complex and high-dimensional dataset, is successfully classified with the help of less learnable parameters. The frame selection and shallow CNN architectures proposed in this study can be adapted for remote sensing applications, where large-scale image data requires efficient processing. By reducing computational demands, our approach facilitates real-time analysis in resource-constrained environments.

An effective preprocessing is one of the main challenges in the MRI data analysis. If the preprocessing pipeline changes according to the MRI data, the model overfitting or underfitting can be avoided. A limitation of this research is that we have followed specific preprocessing steps, such as skull stripping and different normalization and registration methods. In the future, the incorporation of other potential preprocessing approaches for feature extraction and denoising, such as wavelet decomposition and empirical mode decomposition, can be explored. Moreover, the performance of different feature selection algorithms, such as metaheuristic optimizers, will be studied.

Data availability

The ADNI database is publicly available for research purpose and it is composed of the Magnetic Resonance Images (MRIs). This data set is used in this study.

Received: 15 April 2024; Accepted: 7 March 2025

Published online: 18 March 2025

References

- Ulep, M. G., Saraon, S. K. & McLea, S. Alzheimer disease. *J. Nurse Practitioners*. **14** (3), 129–135 (2018).
- Gauthier, S., Webster, C., Servaes, S., Morais, J. & Rosa-Neto, P. *World Alzheimer Report 2022: Life after Diagnosis: Navigating Treatment, Care and Support Ed* (Alzheimer's disease international London, England, 2022).
- Lorio, S. et al. Neurobiological origin of spurious brain morphological changes: A quantitative MRI study. *Hum. Brain. Mapp.* **37** (5), 1801–1815 (2016).
- Arafa, D. A., Moustafa, H. E. D., Ali-Eldin, A. M. & Ali, H. A. Early detection of Alzheimer's disease based on the state-of-the-art deep learning approach: A comprehensive survey. *Multimed. Tools Appl.*, pp. 1–42 (2022).
- Ebrahimighahnavieh, M. A., Luo, S. & Chiong, R. Deep learning to detect Alzheimer's disease from neuroimaging: A systematic literature review. *Comput. Methods Progr. Biomed.* **187**, 105242 (2020).
- Moradi, E., Pepe, A., Gaser, C., Huttunen, H. & Tohka, J. and A. s. D. N. Initiative, Machine learning framework for early MRI-based Alzheimer's conversion prediction in MCI subjects. *Neuroimage* **104**, 398–412 (2015).
- Sharma, S. & Mandal, P. K. A comprehensive report on machine learning-based early detection of Alzheimer's disease using multi-modal neuroimaging data. *ACM Comput. Surv. (CSUR)*. **55** (2), 1–44 (2022).
- Hinrichs, C. et al. Spatially augmented LPboosting for AD classification with evaluations on the ADNI dataset. *Neuroimage* **48** (1), 138–149 (2009).
- Terry, R. D. Alzheimer's disease and the aging brain. *J. Geriatr. Psychiatr. Neurol.* **19** (3), 125–128 (2006).
- Rathore, S., Habes, M., Iftikhar, M. A., Shacklett, A. & Davatzikos, C. A review on neuroimaging-based classification studies and associated feature extraction methods for Alzheimer's disease and its prodromal stages. *NeuroImage* **155**, pp. 530–548 (2017).
- Soydaner, D. Attention mechanism in neural networks: Where it comes and where it goes. *Neural Comput. Appl.* **34** (16), 13371–13385 (2022).
- Li, X. et al. Deep learning attention mechanism in medical image analysis: Basics and beyonds. *Int. J. Netw. Dyn. Intell.*, pp. 93–116 (2023).
- Liu, Z. et al. Diagnosis of Alzheimer's disease via an attention-based multi-scale convolutional neural network. *Knowl. Based Syst.* **238**, 107942 (2022).
- Yadav, B. K. & Hashmi, M. F. An attention-based CNN architecture for Alzheimer's classification and detection. In *2023 IEEE IAS Global Conference on Emerging Technologies (GlobConET)*. IEEE, pp. 1–5 (2023).
- Golovanevsky, M., Eickhoff, C. & Singh, R. Multimodal attention-based deep learning for Alzheimer's disease diagnosis. *J. Am. Med. Inform. Assoc.* **29** (12), 2014–2022 (2022).
- Vincent, P. et al. Stacked denoising autoencoders: Learning useful representations in a deep network with a local denoising criterion. *J. Mach. Learn. Res.*, **11**, 12, (2010).
- Hinton, G. E. Deep belief networks. *Scholarpedia* **4** (5), 5947 (2009).
- Ebrahimi, A. Luo, and F. T. A. S. Disease neuroimaging initiative, convolutional neural networks for Alzheimer's disease detection on MRI images. *J. Med. Imaging*. **8** (2), 024503–024503 (2021).
- Cui, R., Liu, M. & Initiative, A. D. N. RNN-based longitudinal analysis for diagnosis of Alzheimer's disease. *Comput. Med. Imaging Graph.* **73**, 1–10 (2019).
- Sharma, M., Sharma, P., Pachori, R. B. & Acharya, U. R. Dual-tree complex wavelet transform-based features for automated alcoholism identification. *Int. J. Fuzzy Syst.* **20** (4), 1297–1308 (2018).
- Farooq, A., Anwar, S., Awais, M. & Rehman, S. A deep CNN based multi-class classification of Alzheimer's disease using MRI. In *IEEE International Conference on Imaging systems and techniques (IST)*. IEEE, pp. 1–6. (2017).
- Haarburger, C. et al. Multi scale curriculum CNN for context-aware breast MRI malignancy classification. In *International Conference on Medical Image Computing and Computer-Assisted Intervention*. Springer, pp. 495–503 (2019).
- Khagi, B. & Kwon, G. R. 3D CNN design for the classification of Alzheimer's disease using brain MRI and PET. *IEEE Access*. **8**, 217830–217847 (2020).
- Mehmood, A. et al. A transfer learning approach for early diagnosis of Alzheimer's disease on MRI images. *Neuroscience* **460**, 43–52 (2021).
- Acharya, R. M. H. & Singh, D. K. Alzheimer disease classification using transfer learning. In *5th International Conference on Computing Methodologies and Communication (ICCMC)*, pp. 1503–1508 (2021).
- Deepak, S. & Ameer, P. Automated categorization of brain tumor from mri using Cnn features and Svm. *J. Ambient Intell. Humaniz. Comput.* **12** (8), 8357–8369 (2021).
- Shakarami, A., Tarrah, H. & Mahdavi-Hormat, A. A CAD system for diagnosing Alzheimer's disease using 2D slices and an improved AlexNet-SVM method. *Optik* **212**, 164237 (2020).
- Ebrahim, D., Ali-Eldin, A. M., Moustafa, H. E. & Arafat, H. Alzheimer disease early detection using convolutional neural networks. In *15th international conference on computer engineering and systems (ICCES)*. IEEE, pp. 1–6. (2020).
- Yadav, K. S. & Miyapuram, K. P. A novel approach towards early detection of Alzheimer's disease using deep learning on magnetic resonance images. In *International Conference on Brain Informatics*. Springer, pp. 486–495 (2021).
- Buvaneswari, P. & Gayathri, R. Deep learning-based segmentation in classification of Alzheimer's disease. *Arab. J. Sci. Eng.* **46** (6), 5373–5383 (2021).
- Odusami, M., Maskeliūnas, R., Damaševičius, R. & Krilavičius, T. Analysis of features of alzheimer's disease: detection of early stage from functional brain changes in magnetic resonance images using a finetuned ResNet18 network. *Diagnostics* **11**(6), 1071 (2021).
- Prakash, D. et al. Diagnosing Alzheimer's disease based on multiclass MRI scans using transfer learning techniques. *Curr. Med. Imaging*. **17** (12), 1460–1472 (2021).
- Huang, Y., Xu, J., Zhou, Y., Tong, T. & Zhuang, X. S. D. N. Initiative, diagnosis of Alzheimer's disease via multi-modality 3D convolutional neural network. *Front. NeuroSci.* **13**, 509 (2019).
- Solano-Rojas, B., Villalón-Fonseca, R. & Marín-Raventós, G. Alzheimer's disease early detection using a low cost three-dimensional densenet-121 architecture. In *International Conference on Smart Homes and Health Telematics*. Springer, pp. 3–15 (2020).
- Wang, H. et al. Ensemble of 3D densely connected convolutional network for diagnosis of mild cognitive impairment and Alzheimer's disease. *Neurocomputing* **333**, 145–156 (2019).
- Zhang, Z. and Farzad Khalvati. Introducing vision transformer for Alzheimer's disease classification task with 3D input. *arXiv preprint arXiv:2210.01177* (2022).
- Sarraf, S. et al. OViTAD: Optimized vision transformer to predict various stages of Alzheimer's disease using resting-state fMRI and structural MRI data. *Brain Sci.* **13** (2), 260 (2023).
- Han, S. et al. Dsd: Dense-sparse-dense training for deep neural networks, presented at the 5th International Conference on Learning Representations, France (2017).
- Weiner, M. W. et al. The Alzheimer's disease neuroimaging initiative 3: Continued innovation for clinical trial improvement. *Alzheimer's Dement.* **13** (5), 561–571 (2017).
- Mueller, S. G. et al. The Alzheimer's disease neuroimaging initiative. *Neuroimaging Clin.* **15** (4), 869–877 (2005).
- a., R. P. & Toennies, K. D. Segmentation of medical images using adaptive region growing. *Med. Imaging Image Process*, pp. 1337–1346 (2017).
- Ashburner, J. A fast diffeomorphic image registration algorithm. *Neuroimage* **38**, 95–113 (2007).

43. Pan, A. Z. D., Jia, L., Huang, Y., Frizzell, T. & Song, X. Early detection of Alzheimer's disease using magnetic resonance imaging: A novel approach combining convolutional neural networks and ensemble learning. *Front. NeuroSci.*, **14**, (2020).

Acknowledgements

The authors are grateful to Ghulam Ishaq Khan institute of engineering sciences and technology, American University of the Middle East, Effat University, National University of Computer and Emerging Sciences, University of Malaya, Cracow University of Technology, and Polish Academy of Sciences for the technical and logistic support. They are also thankful to the Effat University, Cracow University of Technology, and Polish Academy of Sciences for financially supporting this work.

Author contributions

Conceptualization, Jalees ur Rahman, Muhammad Hanif, Saeed Mian Qaisar, and Usman Haider; Methodology, Jalees ur Rahman, Muhammad Hanif, and Obaid ur Rehman; Implementation, Jalees ur Rahman, and Obaid ur Rehman; Formal analysis, Jalees ur Rahman, Muhammad Hanif, Usman Haider, and Saeed Mian Qaisar; Investigation, Obaid ur Rehman, and Pawel Plawiak; Resources, Saeed Mian Qaisar, Muhammad Hanif, and Pawel Plawiak; Writing—original draft preparation, Jalees ur Rahman, Saeed Mian Qaisar, Obaid ur Rehman, and Usman Haider; Writing—review and editing, Muhammad Hanif, and Pawel Plawiak; Visualization, Jalees ur Rahman, and Obaid ur Rehman; Supervision, Muhammad Hanif, and Saeed Mian Qaisar; Project administration, Saeed Mian Qaisar, and Muhammad Hanif; Funding acquisition, Saeed Mian Qaisar, and Pawel Plawiak. All authors have read and agreed to the published version of the manuscript.

Declarations

Competing interests

The authors declare no competing interests.

Additional information

Correspondence and requests for materials should be addressed to S.M.Q. or P.P.

Reprints and permissions information is available at www.nature.com/reprints.

Publisher's note Springer Nature remains neutral with regard to jurisdictional claims in published maps and institutional affiliations.

Open Access This article is licensed under a Creative Commons Attribution-NonCommercial-NoDerivatives 4.0 International License, which permits any non-commercial use, sharing, distribution and reproduction in any medium or format, as long as you give appropriate credit to the original author(s) and the source, provide a link to the Creative Commons licence, and indicate if you modified the licensed material. You do not have permission under this licence to share adapted material derived from this article or parts of it. The images or other third party material in this article are included in the article's Creative Commons licence, unless indicated otherwise in a credit line to the material. If material is not included in the article's Creative Commons licence and your intended use is not permitted by statutory regulation or exceeds the permitted use, you will need to obtain permission directly from the copyright holder. To view a copy of this licence, visit <http://creativecommons.org/licenses/by-nc-nd/4.0/>.

© The Author(s) 2025